

Forest fire plumes over the North Atlantic: p-TOMCAT model simulations with aircraft and satellite measurements from the ITOP / ICARTT Campaign

Peter Cook ¹, Nick Savage ^{1,2}, Solène Turquety ^{3,4}, Glenn Carver ^{1,2}, Fiona O'Connor ^{1,5}, Andreas Heckel ⁶, Dave Stewart ⁷, Lisa Whalley ⁸, Alex Parker ⁹, Hans Schlager ¹⁰, Hanwant Singh ¹¹, Melody Avery ¹², Glen Sachse ¹², Bill Brune ¹³, Andreas Richter ⁶, John Burrows ⁶, Ruth Purvis ¹⁴, Ally Lewis ¹⁵, Claire Reeves ⁷, Paul Monks ⁹, Oliver Wild ¹, James Levine ¹ and John Pyle ^{1,2}

¹ Centre for Atmospheric Science, Department of Chemistry, University of Cambridge, UK

² NCAS ACMSU, University of Cambridge, UK

³ Atmospheric Chemistry Modeling Group, Harvard University, USA

⁴ Now at Service d' Aéronomie, IPSL, Paris, France

⁵ Now at Meteorological Office, UK

⁶ Institute of Environmental Physics, University of Bremen, Germany

⁷ School of Environmental Sciences, University of East Anglia, UK

⁸ School of Chemistry, University of Leeds, UK

⁹ Department of Chemistry, University of Leicester, UK

¹⁰ Institut fuer Physik der Atmosphaere, Deutsches Zentrum fuer Luft – und Raumfahrt (DLR), Oberpfaffenhofen, Germany

¹¹ NASA Ames RC, Moffett Field, CA, USA

¹² NASA Langley RC, USA

¹³ Pennsylvania State University, USA

¹⁴ Facility of Airborne Atmospheric Measurements, Cranfield, UK

¹⁵ Department of Chemistry, University of York, UK

Abstract

ITOP (Intercontinental Transport of Ozone and Precursors), part of ICARTT (International Consortium for Atmospheric Research on Transport and Transformation), was an intense research effort to measure the long range transport of pollution across the North Atlantic and its impact on O₃ production. During the aircraft campaign in July and August 2004 plumes were encountered containing large concentrations of CO plus other tracers and aerosols emitted from forest fires in Alaska and Canada. A chemical transport model, p-TOMCAT, and new inventories of the biomass burning emissions during May to August 2004 have been used to simulate the plume locations and tracer concentrations from these fires. The simulated plumes closely match CO measurements from the aircraft and also CO data from the MOPITT satellite instrument. Then, by including additional vertical mixing of O₃ into the troposphere above the fires, and using a low NO_x/CO emission ratio for boreal fires, O₃ concentrations in the simulated plumes are reduced closer to the aircraft measurements, with NO₂ closer to SCIAMACHY satellite instrument data, although too little PAN is produced. In the p-TOMCAT simulations the fire emissions lead to increased O₃ in the troposphere over much of North America, the north Atlantic and western Europe from photochemical production and transport. The increased O₃ over the northern hemisphere reaches a peak in the range 2.0 to 6.2 Tg.

1. Introduction

In recent years a number of campaigns have studied the long range transport of air pollution and its impact on O_3 production, including NARE (North Atlantic Regional Experiment) and OCTA (Oxidizing Capacity of the Tropospheric Atmosphere) in 1993 [e.g., Wild et al. 1996]. The transpacific transport of pollution, including boreal fire emissions, was examined in the ITCT 2002 (Intercontinental Transport and Chemical Transformation), PHOBEA (Photochemical Ozone Budget of the Eastern North Pacific Atmosphere) and PEACE-B (Pacific Exploration of Asian Continental Emission) campaigns [e.g. Bertschi et al. 2004; Hudman et al. 2004]. Intercontinental transport of pollution remains a major research theme. In this context ICARTT (International Consortium for Atmospheric Research on Transport and Transformation) was a large international project involving groups from the USA, Canada, France, Germany, the UK and Portugal. It was composed of smaller national projects including ITOP, INTEX-NA, ITCT-2K4 and NEAQS. The aim was to study the long range influence of pollutants (such as CO and NO_x) from North America, and the production and transport of O_3 in the troposphere. A variety of atmospheric measurements were made over North America, the North Atlantic and Europe during intensive field campaigns between June and August 2004, including remote sensing from satellite instruments (for further details see the overview of ICARTT in Fehsenfeld et al. [2006]). ICARTT used research aircraft to make in-situ measurements of a range of trace gases in July and August 2004. The NASA DC8 aircraft and the NOAA P3 aircraft flew from the US east coast (part of INTEX-NA), while the UK BAe-146 research aircraft was based in the Azores and the DLR Falcon aircraft was based at Creil, France (part of ITOP).

Central to the observational strategy of ICARTT were attempts to observe the same air mass over several days using the different aircraft in order to measure the chemical aging of polluted air. In an earlier study Methven et al. [2003] used the Reverse Domain Filling (RDF) method to follow the trajectories of air masses over the North Atlantic and match flight data to particular air masses by their equivalent potential

temperature and specific humidity. Here by using back trajectories Methven et al. [2006] identified those air masses which were intercepted by two or more flights during the ICARTT campaign.

Although the primary objective of the project was to observe long range transport of anthropogenic pollution from North America, during the campaign the aircraft also encountered the plumes from huge forest fires which burned in Alaska and west Canada between June and September 2004 emitting large quantities of CO and other species (see IGAC Newsletter, issue 32, November 2005). An especially intense fire plume was measured by the DC8 on the 18th July, by the BAe-146 on the 20th (when CO was measured at over 500 ppbv and a brown haze was visible), and then by the DLR Falcon on the 23rd. Figure 1 shows the 3D trajectory of this plume and the three flight tracks.

Biomass burning is a major source of trace gases in the troposphere but is highly variable in space and time and so is a significant factor in the inter-annual variability of atmospheric composition. Each year forest fires in many regions of the world emit 171-561 Tg of CO, 2.4-5.0 Tg N of NO_x and a variety of other gases and aerosols [Schultz et al. 2006]. Biomass burning emissions can travel thousands of kilometers and cover extensive regions, especially when the heat from the fires creates pyro-convective plumes that can reach the upper troposphere and lower stratosphere [Fromm et al. 2005]. CO is a major precursor of O₃ production so biomass burning can have a large impact on tropospheric pollution and O₃ budgets over large regions, leading to enhanced CO and O₃ at the surface a long way downwind of the burning regions.

One of the largest biomass burning events of the 20th century was associated with the Indonesian wildfires of September to November 1997 with estimated emissions of 124 Tg of CO and 2.6 Tg N of NO_x [Duncan et al. 2003a]. Model results including the fire emissions better reproduce observed CO over the Seychelles, Australia and Hawaii, and observed O₃ over Java, Samoa and Tahiti [Duncan et al. 2003b]. Boreal fire emissions were examined by Wofsy et al. [1992], Wotawa and Trainer [2000] and McKeen et al. [2002].

Wotawa and Trainer estimated that Canadian forest fires emitted 12 Tg of CO between mid June to mid July 1995, exceeding the total anthropogenic CO emissions for North America during this period by a factor of 2. However all three studies found that boreal fires have much lower NO_x/CO emission ratios than tropical fires, and less associated O₃ production.

This paper seeks to investigate whether the fires in Alaska in 2004 were only of regional importance or had an impact on a wider, even hemispheric scale. The global chemistry-transport model p-TOMCAT was run with new daily inventories of biomass burning emissions [Turquety et al. 2006], in which the Alaskan and west Canadian forest fires emitted 27 Tg of CO, (which includes 9 Tg of CO from peat burning), and 0.5 Tg N of NO_x during June to August 2004. Figure 2 shows the daily emissions of CO from these fires in the new inventories, with the largest peak in mid July responsible for the intense fire plume measured by the aircraft (figure 1). These estimates are in good agreement with Pfister et al. [2005] who used satellite observations in a top-down inverse analysis to optimize the CO emissions from the fires, finding a best estimate of 30 +/- 5 Tg. This inventory in the chemical transport model allows us to simulate the fire plume locations and the concentrations of CO and other trace gases. We examine the changes in atmospheric composition resulting from the forest fires in Alaska and west Canada, including the impact on O₃ production in the troposphere and pollution and O₃ levels over North America, the North Atlantic and Europe.

Section 2 describes the aircraft observations and the satellite instrument data. Section 3 describes p-TOMCAT and its output, the inventories of the biomass burning emissions, and the four model simulations used. Section 4.1 compares the modeled CO to the satellite and aircraft measurements to examine the model transport. Section 4.2 compares the modeled O₃, NO_x, PAN and HO₂ to measurements to examine the chemistry in the plumes. Section 4.3 uses the model simulations to examine the impact of the fire emissions on global and regional tropospheric O₃, while section 4.4 examines enhancements in surface CO and O₃ over the UK. Conclusions are drawn in section 5.

2. Observations

2.1 Aircraft Observations

The aircraft provided extensive measurements of a wide variety of trace gases. In this study we use measurements of CO, O₃, NO, PAN and peroxy radicals (HO₂+RO₂) from the BAe-146, measurements of CO, O₃, NO, PAN, NO₂, HNO₃ and HO₂ from the DC8, and measurements of CO, O₃, NO and NO_y from the DLR Falcon.

On the BAe-146, CO was measured using an aerolaser UV monitor with 10s integration and 2 ppbv detection limit [Gerbig et al. 1999] and O₃ by a thermo environmental (TECO 49) UV photometric instrument. NO was measured by chemiluminescence with in-flight sensitivity checks using a standard concentration of NO [Brough et al. 2003] and PAN by using a custom built gas chromatograph with electron capture detection (GC-ECD) with 90s integration, 5 pptv detection limit and pre-flight calibration [Whalley et al. 2004]. HO₂+RO₂ was measured using a peroxy radical chemical amplifier (PERCA) [Green et al. 2006].

On the DC8, NO₂ was measured using laser induced fluorescence (LIF) with a detection sensitivity of 0.8 ppt/min at S/N=2 and an uncertainty in the instrument zero of less than 1 ppt [Cleary et al. 2002]. All the instruments on the DC8 are described by Singh et al. [2006].

On the DLR Falcon, CO was measured with an upgraded aerolaser vacuum UV fluorescence instrument [Gerbig et al. 1999] with a time integration of 5s and an accuracy of 5%. O₃ was measured with a UV absorption technique (Thermo Electron TE49) also with 5s time integration and 5% accuracy. The measurement of NO and NO_y was based on a NO-O₃-chemiluminescence technique [Schlager et al. 1999], 1s

time integration with accuracy of 7% (NO) and 12% (NO_y). In the NO_y measurement channel reactive nitrogen species were reduced to NO before detection using a heated gold converter.

2.2 Satellite data

Profiles of CO in the troposphere were measured remotely by the MOPITT (Measurement Of Pollution In The Troposphere) instrument on the EOS-Aura satellite [Drummond and Mand, 1996, Edwards et al. 1999]. This data is available to download from the web site of the NCAR MOPITT Team. Satellite remote sensing measurements of a wide range of trace gases were made by the SCIAMACHY (SCanning Imaging Absorption spectroMeter for Atmospheric CHartographY) instrument [Bovensmann, 1999] on the ENVISAT satellite during the campaign period. SCIAMACHY is a passive remote sensing instrument measuring back scattered Earth radiance and extraterrestrial irradiance in the UV, visible and near IR wavelength range. The NO₂ retrieval is based on a DOAS fit using the spectral window from 425nm to 450nm [Richter and Burrows 2002]. The stratospheric part of the column was removed by the reference sector method: measurements from the Pacific sector (170°-210° E) are assumed to have no tropospheric NO₂ and are subtracted from the other measurements at each latitude. Only pixels with a cloud cover less than 10% were used. A more detailed description regarding the air mass factors applied in the retrieval can be found in Richter et al. [2005].

3. The p-TOMCAT model

3.1 Model description

The model used in this study is the global offline chemistry transport model p-TOMCAT. It is an updated version [see O'Connor et al., 2005] of a model previously used for a range of tropospheric chemistry studies [Savage et al. 2004, Law et al. 2000, Law et al. 1998]. Tracer advection was calculated with the second

order moments advection scheme of Prather [1986] as implemented by Chipperfield [1996] with a 30 minute time step. Convective transport was based on the mass flux parameterisation of Tiedke [1989]. The parameterisation includes parameterised deep and shallow convection with convective updrafts and large-scale subsidence, as well as turbulent and organised entrainment and detrainment. The model contains a non-local vertical diffusion scheme based on the parameterisation of Holtslag and Boville [1993]; for details of the scheme implementation see Wang et al [1999].

In this study p-TOMCAT was run with a $2.8^{\circ} \times 2.8^{\circ}$ horizontal resolution and 31 vertical levels from the surface to 10hPa. The offline meteorological fields used are from the operational analyses of European Medium Range Weather Forecast model. The model represents the transport and chemistry of 42 chemical compounds including tracers of stratospheric ozone and nitrogen oxides, of which 32 tracers are advected. The chemical mechanism includes the chemistry of methane, ethane and propane plus their oxidation products and includes 89 bimolecular, 16 termolecular and 27 photolysis reactions. The model chemistry uses the atmospheric chemistry integration package ASAD [Carver et al. 1997] and is integrated with the IMPACT scheme of Carver and Stott [2000]. The ozone and nitrogen oxide concentrations at the top model level are constrained to zonal mean values calculated by the Cambridge 2D model [Law and Nisbet 1996]. The chemical rate coefficients used by p-TOMCAT have been recently updated to those in the IUPAC Summary of March 2005.

The model parameterisations of wet and dry deposition are described in Giannakopoulos et al. [1999]. Anthropogenic emissions of NO_x , CO, and NMHCs are based on the values used in the Oxcomp model intercomparison [Gauss et al. 2003]. Lightning emissions use the parameterisation of Price and Rind [1992] as implemented by Stockwell et al [1999] with total emissions of 5 Tg (N) yr^{-1} . For more details of the emissions see O'Connor et al [2004]. The standard model version uses a monthly mean climatology for the distribution of biomass burning emissions based on the seasonal distribution of Hao and Liu [1994] and

annual totals from the IPCC Oxcomp [Gauss et al. 2003]. This version of the model was spun up from 1st January 2003 to 1st May 2004.

3.2 Model outputs

As well as the standard model output of three dimensional fields for the tracers of interest at 30 minute intervals, extra outputs were used to investigate the model comparison to aircraft and satellite data, and the ozone budget. Tracer fields were interpolated in space to the aircraft position on-line in the model (data at 10 second intervals) within each time step to compare the model simulations to the aircraft measurements. For comparisons to satellite data the 3D fields of CO and NO₂ are output from the model at the 10:30 local time overpass. Tropospheric columns of NO₂ were calculated by the reference sector method (see section 2.2). However the exact method of subtracting the stratospheric column has little impact on the model agreement with the satellite data [Savage et al, 2004] Burdens of CO, O₃ and other trace gases within a given region can be calculated from the 3D tracer fields.

Finally an ozone budget code based on that described in O'Connor et al [2004] was used. Fields of the contributions to the ozone budget due to different chemical processes, vertical transport and dry deposition are all output to allow the O₃ budget within different regions of the atmosphere to be examined.

3.3 Biomass burning emissions

The standard biomass burning emissions used in p-TOMCAT, with a seasonal variation based on Hao and Liu [1994], contain monthly mean values for an ‘average’ year. This implies that specific events such as the fires which are of interest in this study cannot be accurately represented. To investigate the Alaskan and Canadian wildfires a new emission inventory for biomass burning has been exploited.

For North America, daily mean emissions of CO, NO₂, formaldehyde, ethane, propane, acetaldehyde and acetone were provided at 1° x 1° resolution. These emissions were calculated using MODIS hotspot data, reported area burned, and information on type of vegetation, fuel loading and emission factors [for more details see Turquety et al. 2006]. The biomass burning emissions for the rest of the world during this period were based on the Yevich and Logan [2003] inventory, also provided at 1° x 1° resolution, and are monthly mean climatologies not daily data. All the emission inventories were re-gridded to 2.8° x 2.8° resolution for p-TOMCAT. Global CO emissions in the new inventory are smaller with only 156 Tg of CO emitted during May to August 2004, whereas the emissions in the same period from the standard emissions is 249 Tg of CO. Following the model spin up with the standard model set up, the new inventory was used from 1st May 2004 for all the studies described in this paper.

3.4 Model simulations performed

Four model simulations were performed (see table 1). The first (run A) excluded the biomass burning emissions from the Alaska and west Canada fires (the region 80.2°-170.2° W and 55.8°-75.3° N, see rectangular box in figure 3) to provide a baseline. The other runs all included the fire emissions from the Alaska and west Canada region (CO, NO₂, formaldehyde, ethane, propane, acetaldehyde and acetone). In the inventories the emissions are only from small areas within this region, and the locations of these changed from day to day.

The Alaska and west Canada fires generated powerful pyro-convection which carried the emissions high into the troposphere, and commercial aircraft observed plumes reaching the tropopause (see the photograph in the IGAC Newsletter, issue 32, November 2005). Damoah et al. [2006] have also identified pyro-convective events for the Alaska and west Canada fires. We suspect that for strong fires, there will be substantial lofting

of the boundary layer air, with low O_3 , and we have attempted to describe this simply in 2 different ways. In run B the emissions were placed uniformly into the troposphere (constant mixing ratio) between the surface and 260 hPa altitude, about 10 km. The third simulation (run C) placed all the fire emissions at the surface, then additional vertical mixing was applied to the emission tracers, and also O_3 , to produce a uniform profile of these species between the surface and 260 hPa. This mixing was done every time step, within the Alaska and west Canada region, where the emissions increased surface concentrations of CO by more than 20%. For smaller fires with fewer emissions the CO and other tracers were given no additional vertical mixing and remained near to the surface. The homogenization of the model profiles over the fires in this simulation is not meant to be an accurate representation of pyro-convection but instead represents a sensitivity study on the impact of the redistribution of tropospheric O_3 . In all four simulations the biomass burning emissions in all other regions were confined to the surface and had no additional vertical mixing.

The NO_x/CO emission ratio for the Alaska and west Canada fires in the new inventory is typical of tropical biomass burning [Duncan et al. 2003a] but boreal fires have a much lower ratio [Wofsy et al. 1992; Bertschi et al. 2004]. Therefore a fourth model simulation (run D) was carried out with NO_2 emissions from the Alaska and west Canada fires reduced by a factor of 4. This reduction was to match the NO_x/CO emission ratio of 0.007 found by McKeen et al. [2002] by using model simulations of O_3 production and also measurements of NO_y . Vertical mixing over the fires was also applied, as in run C, to study the model sensitivity to both reduced NO_x and vertical mixing of O_3 . The results from the different simulations were then compared to examine the impact of the forest fires on the tracer fields and ozone budgets over North America, the North Atlantic and Western Europe.

4. Results

4.1 CO in the fire plumes

Figure 3 shows the CO tracer field from p-TOMCAT for model run D and the increases between runs A and D at 500 hPa on the 20th July 2004 (12:00 UT), with the region which includes the Alaskan and west Canadian forest fires shown by a rectangle. The CO field shows a line of fire plumes right across Canada and the North Atlantic at 500 hPa from the fire emissions, and increases in CO are also seen over the east coast of the USA, Greenland and Iceland.

Figure 4 compares model run D to measurements of CO columns from the MOPITT satellite instrument. The measurements of CO are quite patchy as the EOS-Aura satellite only covers about half the globe each day (at 60° N) and pixels with more than 10% cloud cover are rejected. So here the combined measurements from the 19th, 20th and 21st July 2004 are calculated and then compared to the mean of the model columns at 10:30 local time on the same three days from the simulation. The CO simulated by p-TOMCAT in the fire plumes over Alaska, Canada and the North Atlantic, and also over Central Africa, is clearly seen in the MOPITT measurements at the same locations. Directly comparing the model simulations to the measurements by averaging over the larger model pixels produces an orthogonal least-squares fit of gradient 0.55 for run A and 0.93 for run D. The regression coefficient is increased from 0.52 to 0.64 between runs A and D, and the model fire plumes are a good match to the MOPITT measurements in magnitude and location. (Pfister et al. [2005] also found model plumes in the same locations as MOPITT data).

Figure 5 shows profiles of the measurements of CO from the three flights which encountered the large fire plume. To create this profile mean values in 25 hPa bins were calculated. The plume is clearly seen in the large CO values around 400 hPa measured from the DC8 on the 18th July, between 600-400 hPa from the BAe-146 on the 20th, and 550-475 hPa from the DLR Falcon on the 23rd (with enhanced CO values down to 825 hPa). These are compared to the mean values from the four model simulations. The model CO values with the fire emissions are much larger, particularly at the plume altitudes, and match the measurements quite closely, although over Europe the model profiles have little structure. Detailed investigation of the model 3D

tracer fields shows considerable vertical mixing of the fire plume when it reaches the west coast of Europe on the 22nd July. The increasing vertical distribution of the measurements is evidence of substantial mixing in the actual atmosphere, though not as much as in the model simulations. These results shown in figures 3, 4 and 5 suggest that the model has captured quite accurately the plumes in terms of location, altitude and magnitude and that the new CO emissions for the fires are realistic. Other researchers including Wotawa and Trainer [2000], McKeen et al. [2002] and Duncan et al. [2003b] have also put CO emissions from fires into models and obtained results much closer to measurements.

4.2 Chemistry in the fire plumes

Figure 6 shows the model O₃ and NO_x fields from run D and the increase between runs A and D at 500 hPa on the 20th July (12:00 UT). The region containing the Alaskan and west Canadian fires is shown by the rectangle. The fire emissions produce a line of plumes across Alaska, Canada and the North Atlantic, very similar to those for CO in figure 3, plus enhanced NO_x over the east coast of the USA. Further south there are large regions of reduced O₃ resulting from the additional vertical mixing of O₃ in run D.

Figure 7 compares the measurements of NO₂ tropospheric columns from the SCIAMACHY satellite instrument to model columns from run D. The coverage of NO₂ from the ENVISAT satellite is incomplete, as with MOPITT on EOS-Aura, and also SCIAMACHY alternates between nadir (for columns) and limb sounding. So as with CO the measurements and model columns from 3 days are combined. Estimates of the NO₂ in the stratosphere have been subtracted at each model latitude band to match the processing of the measurements.

Both the measurements and model results show enhanced NO₂ across Canada and the North Atlantic, but the fire plumes are much less pronounced than for CO. Also the model values over land are too large. This is

consistent with Savage et al. [2004] in which NO_2 columns from the GOME instrument were compared to TOMCAT results finding a good overall correlation, but model columns were too large over polluted areas probably due to weaknesses in model vertical mixing and chemistry. When the model simulations here are compared directly to the measurements from the 3 days, by averaging the measurements over the larger model pixels, the gradient of the orthogonal least-squares fit is 2.77 for run A and 2.74 for run D and the regression coefficient is slightly reduced from 0.56 to 0.54. The large gradients are due to the large model values of NO_2 over land, and the slightly better fit with no emissions suggests that there was little NO_2 within the actual fire plumes. So either the NO_2 emissions are indeed too great in the biomass burning inventories, or most of the NO_2 emitted was rapidly removed or converted to PAN, or some combination of these. In the model simulations NO_x within the fire plumes is seriously overestimated if we do not reduce the NO_2 emissions.

Figure 8 shows the vertical profile of NO, O_3 , PAN and NO_y (ppbv) measured on the three flights which encountered the large fire plume, again with mean values calculated in 25 hPa bins and compared to the four model simulations. The DC8 measurements of NO_y here are the sum of the NO, NO_2 , PAN and HNO_3 measurements from this flight. There were no NO_y measurements from the BAe-146 flight and no PAN measurements from the DLR Falcon flight

Unlike for CO, no clear plume is seen in the NO observed by any of the three flights. In contrast for model runs B and C the modeled concentrations of NO for the DC8 and BAe-146 show enhanced concentrations at the same altitude as the peak concentrations of CO (figure 5). The NO concentrations in runs A and D match the observed profiles of NO much better. This strongly indicates that the NO_x/CO ratio in the original emission inventory was much too high and the NO_x/CO emission ratio of 0.007 found by McKeen et al. [2002] matches these fires more closely. For the DLR Falcon flight over France the four model runs give very similar results for NO indicating that after a few days the modeled impact of the fires on the NO profiles

here is small. In addition all the model runs have higher NO concentrations than the observations. Detailed investigation of the model 3D tracer fields for the 23rd July shows vertical mixing in the model bringing up NO_x from the surface and also bringing down NO_x from the stratosphere.

The effect of NO on ozone can be seen for both the observations and the four model runs. For the DC8 flight the measurements of O₃ show no enhancement at altitudes around 400 hPa - in fact, O₃ was slightly reduced. This suggests that there was very low ozone production rates or even slight ozone destruction in this part of the plume. For the BAe-146 and DLR Falcon flights there are some enhancements in observed ozone but these are smaller than those seen for CO. In general the DC8 ozone profile is reproduced well by all the model runs but there is a larger peak in runs B and C which is not observed. As with the NO measurements, model runs A and D give much better comparison to the observations although none of the model runs capture the small decrease at the altitude of the plume. A similar picture is seen for the BAe-146 flight with a large overestimate of the ozone concentrations in the plume for runs B and C (though run C with additional vertical mixing reduces the peak in model O₃) and much better agreement for runs A and D. This is consistent with the results of Wofsy et al. [1992] and Bertschi et al. [2004] who also measured low O₃/CO ratios in boreal fire plumes, and McKeen et al. [2002] who found that O₃ production in model plumes is very sensitive to NO_x. It strengthens the case that the lower NO_x emissions from these fires are more accurate. The agreement with the ozone observations made by the DLR Falcon is much poorer for all runs, with, as for NO, a profile completely different from that observed. As mentioned earlier this is probably a result of too much vertical mixing of the plume in the model as it gets close to the coast of Europe. However it is important to note the very large difference in the total ozone in the column between the 4 model runs: run C where ozone is mixed as well as the emissions has lower ozone than run B, and run D has even lower ozone. We can therefore conclude that both the pyro-convective mixing and NO_x/CO ratio of wildfires can have a large impact on the ozone budget.

There are also peaks in the measured PAN and NO_y at the same height as the CO plume for the DC8 profiles and in PAN in the BAe-146 and NO_y in the DLR Falcon measurements. For the DC8 measurements the NO_y is too high in runs B and C which shows that the reason for their excessive NO concentrations is not simply due to incorrect partitioning of NO_y. The peak in model NO_y for run D is much closer to the observations but is somewhat on the low side. This is consistent with the low concentration of PAN compared to observations seen for all the model runs with the fires (B,C and D). Although there is far more NO_x in model runs B and C than in run D there is very little difference in the PAN concentrations. Therefore it seems likely that the low PAN production in all the model simulations may be due to too little acetaldehyde (CH₃CHO), which is oxidized to CH₃C(O)O₂ and then combines with NO₂ to form PAN. The biomass burning emissions inventories contain 5 Tg/yr but there may be too little acetaldehyde from other sources. Acetaldehyde is also produced by the breakdown of higher hydrocarbons such as isoprene which was not included in the chemical mechanism used for these runs. These low model PAN concentrations are also seen the BAe-146 profile and in the lack of NO_y compared to the measurements made by the DLR Falcon.

For the DLR Falcon flight the simulations have too little NO_y even with the fire emissions so most of the model NO_y has been removed before the plume reached Europe. With little PAN formation in the model plume most of the NO_x was converted to HNO₃ instead, and this was washed out before reaching Europe. Also model NO_y is too great near to the surface in all four simulations, implying that the anthropogenic emissions may also be too great in the model or that NO_y is not being removed quickly enough.

To examine further the chemistry within the fire plume the measurements of HO₂ from the DC8 flight and total peroxy radicals (HO₂+RO₂) from the BAe-146 flight are plotted in Figure 9 along with the results from all four model simulations. For the DC8 profile the model results are generally in very good agreement with the observations. The general shape of the profile is reproduced by the model runs and a rapid decrease in the concentrations at about 700 hPa is seen in both the observations and the model runs. In the plume

however model runs B and C show a strong decrease in HO_2 which is not seen in the observations. This is due to the large increase in NO at this altitude in these model runs which will alter the partitioning of HO_x away from HO_2 and towards OH. The much better agreement for run D gives further evidence that the lower NO_x emissions in run D are more accurate.

The modeled peroxy radical profiles from the BAe-146 are in much worse agreement than the HO_2 profiles from the DC8. There is little difference between the four simulations even at the height of the plume. Below about 775 hPa the modeled radical concentrations are lower than those observed while above about 625 hPa they are higher. This might be explained by a cloud layer between 775 and 625 hPa which would enhance radiation above the cloud and lower it below, thus reducing the primary production of OH below the cloud and so causing all radicals to have lower concentrations. This would not be captured in the model which uses cloudiness values from a climatology. Another possible reason might be an incorrect vertical distribution of hydrocarbons in the model. These could form peroxy radicals via reaction with OH or by photolysis for compounds such as acetone and formaldehyde.

We have shown that model O_3 is sensitive to the additional vertical mixing (run C) and to the amount of NO_x (run D), with more NO_x producing more O_3 , although the relationship is not linear since the chemical production of O_3 is more efficient at low NO_x concentrations. In model run D the O_3 and NO values within the fire plume are closest to the aircraft measurements, but model PAN is much too low. Additional PAN would decompose further downwind to release NO_x and produce more O_3 , possibly explaining some of the enhanced O_3 observed by the DLR Falcon over Europe. PAN can transport NO_x over large distances and then release it in regions with greater ozone production efficiency. Hence, due to the reduced PAN, run D represents a low estimate for the increased O_3 resulting from the Alaskan and west Canadian fire emissions. However in model runs B and C, with higher NO_x emissions, the O_3 , NO and NO_y values within the fire

plume are much larger than the aircraft measurements. Runs B and C represent high estimates of the increased O_3 resulting from the fire emissions.

4.3 Modelled impact of fire emissions on northern hemisphere tropospheric ozone

In this section we compare the four model simulations to examine the increase in the tropospheric burden of CO and NO_x due to the Alaska and west Canada fires over selected regions of the northern hemisphere, and the resulting increase in the model O_3 burden. By examining the differences between run A and the three other runs we can study the sensitivity of the O_3 budget to additional vertical mixing of O_3 and to the amount of NO_x emitted. Figure 10 shows the difference between simulations A and D in the model net chemical production and in the dry deposition of O_3 in the lower and middle troposphere, from the surface to ~260 hPa, during the 20th July 2004. Increased O_3 production is seen over Alaska, Canada and the North Atlantic, which matches the patterns of increased CO and NO_x in figures 3 and 6. Increased dry deposition occurs in Alaska, Canada, the Eastern USA, Western Europe and North Africa. There are also large regions of increased O_3 destruction over parts of Alaska and Canada, due to the additional vertical mixing increasing O_3 near to the surface, which is also responsible for most of the increased dry deposition in Alaska and Canada. It is clear that the fire emissions and additional vertical mixing change the photochemical environment over large regions of the model troposphere, implying that forest fires can have a significant short term impact on pollution in the global free troposphere.

The increased production, loss and burden of O_3 within the model northern hemisphere lower and middle troposphere resulting from the fire emissions is now examined in detail. The top panels of figure 11 show the increased burdens of CO (Tg), NO_x (Gg N) and O_3 (Tg) in the whole of the model northern hemisphere troposphere resulting from the fire emissions; the bottom panels show the increased production and loss of O_3 (Tg). The values are the differences between model runs B, C and D and run A during 50 days from 15th

June to 3rd August 2004. NO_x in the model has a strong signal for each of the different episodes of fire emissions in the new inventories (figure 2) while the longer lived CO and O_3 rise and then fall more slowly in the model runs.

Model run B has the largest increases in CO, NO_x and O_3 . The increases are not so great in runs C and D where additional vertical mixing changes the O_3 profile. O_3 is reduced at higher altitudes leading to increased net chemical production of O_3 , while O_3 is increased near the surface leading to increased net chemical destruction and dry deposition of O_3 and also more rapid chemical destruction of CO and NO_x . Between runs B and C the increase in net chemical production of O_3 over the 50 days is greater overall (+11.1 to +12.3 Tg), however dry deposition is also greater (-5.8 to -8.5 Tg) and the peak in the increased O_3 , on the 21st July, is reduced by almost a third by the additional vertical mixing (9.0 to 6.2 Tg).

Run D with low NO_x emissions has a smaller increase in net O_3 production (+7.2 Tg) and more CO remains. Dry deposition is again large (-5.7 Tg) due to vertical mixing giving higher O_3 concentrations at the surface. The peak in increased O_3 is reduced by two thirds by the lower NO_x emissions and occurs later (2.0 Tg on the 31st July). Note that O_3 production seems to be more efficient in run D where although NO_x emissions have been reduced by a factor of 4 the resulting increase in O_3 is only reduced by a factor of 3. In section 4.2 runs B and C were seen to give high estimates for the total O_3 produced by the fire emissions while run D gave a low estimate, so the increase in the O_3 burden over the northern hemisphere is in the range 2.0 to 6.2 Tg.

We now consider three regions of equal area, the eastern USA, the mid Atlantic and western Europe. The upper panels of figure 12 show the increase in CO and O_3 burdens (Tg) between model runs A and D within these three regions of the lower and middle troposphere during the 50 days. With the prevailing west to east wind there is a time delay of about 2 days between the regions, so on the plots the values from the mid Atlantic have been advanced by 2 days and the values for western Europe by 4 days to help with the

comparisons. The lower panels show the increased production and loss of O₃ (Tg) between runs A and D within the eastern USA and western Europe regions due to net chemistry, transport from/to other regions, and dry deposition.

The increases in CO and O₃ rise and fall within each region as the plumes from different episodes of the fire emissions enter and leave. Some of the air masses have reduced O₃ compared to the baseline run A, due to the additional vertical mixing redistributing O₃ and leading to increased dry deposition, and this is particularly seen at the start of the period. Over the first 20 days in the eastern USA region (24 days in the western Europe region) the increases in the CO and O₃ burdens and in net chemical production and dry deposition of O₃ are small, but after this time they become much greater with further increases from large episodes of pollution. While the emissions increase over the first 20 days (figure 2) the greater increases after this time may also be from the meteorology bringing more of the emissions to the three regions. The increased burdens of CO and O₃ peak on the 18th July over the eastern USA, on the 20th over the mid Atlantic and on the 22nd over western Europe which coincides with the track of the intense fire plume.

The additional burdens of CO and O₃ from the fires decline from west to east (highest in the eastern USA and lowest in western Europe) due to a combination of photochemistry and mixing. The increase in net chemical production and dry deposition of O₃ also declines from west to east. However the increased net chemical production of O₃ remains quite large over western Europe and still gives a large increase in the O₃ burden even with both transport and dry deposition removing O₃. The increase in the O₃ burden is very similar within the eastern USA and western Europe regions, peaking at 0.37 and 0.27 Tg respectively and with a final increase due to the fires of 0.21 (eastern USA) and 0.16 Tg (western Europe), even though western Europe is much further from the fires. These results from model run D are perhaps low estimates for the amount of O₃ produced from the fire emissions (since run D has too little PAN compared with observations) suggesting that the actual increase in the O₃ burden over western Europe was even greater.

4.4 Surface CO and ozone

Finally the impact on composition at the surface resulting from the fire emissions is examined. Figure 13 shows the increase in model CO and O₃ at the surface, between runs A and D, which is greatest over western Europe on 22nd July 2004 (see figure 12). Increased surface CO and O₃ is seen over large regions of the northern hemisphere, and parts of the UK have model increases in CO and O₃ over 60 ppbv and 6 ppbv respectively. However we noted earlier that the model simulations are consistent with considerable vertical mixing over the west coast of Europe, bringing tracers from the intense fire plume down to the surface, so that the surface enhancements in CO and O₃ here are probably too great.

Model results for surface CO and O₃ in the UK were compared to observations to look for any impacts on surface pollution from the fire emissions (figure 14). Measurements of CO and O₃ were obtained from the web site of the UK National Air Quality Information Archive. The hourly mean CO values from 16 coastal urban sites and O₃ values from 15 coastal or rural sites were obtained (to try to avoid local urban pollution) and daily minima calculated to look for enhancements in the background CO and O₃. These are compared to mean model values from runs A and D for the UK. Measured CO is generally higher than in the model simulations probably because of the impact of local urban pollution, while measured O₃ is generally lower than in the model.

The measurements show an enhancement in the background CO of about 20 ppbv on the 22nd and 23rd July 2004, at the time that the intense fire plume was over western Europe. The increase in the model surface values of CO between runs A and D is greatest at about 56 ppbv on the 21st and 22nd July which coincides with the observations quite well. The low values in run A at this time may be from the vertical mixing over

the west coast of Europe bringing cleaner air down to the surface, and the high values in run D arise from the vertical mixing bringing down polluted air from the fire plume.

The measurements do not show an obvious enhancement in background O_3 on the 22nd and 23rd July, and there are only small increases in the model surface values of O_3 between runs A and D, greatest at about 6 ppbv on the 21st and 22nd July. Both model runs show enhanced O_3 for the 21st to 23rd July, probably from the vertical mixing over the west coast of Europe bringing down air from the upper troposphere.

The observations may therefore show increased background CO from the fire plume. However finding a fire plume signal in the surface O_3 measurements is more difficult because of the much smaller enhancement expected.

5 Conclusions

By using new inventories of biomass burning emissions during the period May to August 2004 in p-TOMCAT the CO plumes from the large forest fires in Alaska and west Canada can be accurately reproduced in location, altitude and magnitude. The model CO fields from simulations with the fire emissions closely match MOPITT satellite measurements and aircraft measurements from the ITOP campaign, lending support to the meteorology data and to the new inventories.

Model O_3 concentrations are too great within the plumes, although the values are partly reduced by applying additional vertical mixing of the tropospheric O_3 columns above the fires. There is evidence that considerable pyro-convective lofting of boundary layer air into the free troposphere took place above the fires. O_3 in the model plume is then further reduced by decreasing the NO_x emissions from the fires so that O_3 production is decreased. Boreal fires are different from tropical fires in having lower NO_x/CO emission

ratios and a rapid conversion of NO_x to PAN within the plumes, and O_3 production depends critically on the NO_x/CO ratio. By including the additional vertical mixing and decreasing the NO_x emissions the NO_x and O_3 in the model plumes is much closer to the aircraft measurements and to the SCIAMACHY satellite measurements. The model calculations support a low NO_x/CO ratio in these emissions.

However too little PAN was produced in the simulations, probably because of too few higher hydrocarbons in the model. The complex chemistry within the fire plumes is difficult to simulate. Probably the small scale of the plumes and the detailed chemistry within them cannot be fully represented in a global CTM, and the details in the model results are limited by the low spatial resolution. The model simulates the chemistry in the background troposphere more accurately.

The model simulations indicate that the fire emissions lead to a significant increase in tropospheric O_3 over the northern hemisphere, even over western Europe. However the additional vertical mixing of O_3 above the fires reduces the peak model increase in the northern hemisphere tropospheric O_3 burden by almost a third from 9.0 to 6.2 Tg, then decreasing the NO_x emissions from the fires reduces the peak model increase by a further two thirds to 2.0 Tg.

Model runs B and C give too high estimates for the O_3 production as these have too much NO and NO_y within the fire plume, but model run D gives too low an estimate for the O_3 production since it has too little PAN which would decompose releasing further NO_x . So the model simulations suggest that the O_3 produced by the fire emissions in the northern hemisphere troposphere would have reached a peak between 2.0 and 6.2 Tg.

Also the impact of the fires may have been seen in the surface observations of background CO in the UK where both the model and observations show an increase of 20 ppbv. The modeled increase of ozone at the surface is very small (a few ppbv) and is undetectable in the observations.

Acknowledgements

We wish to thank the following: NERC for funding the ITOP Program, their support of NCAS-ACMSU and for supercomputer resources; Paul Young for further development of p-TOMCAT; Ronald C. Cohen and Jack E. Dibb for providing the NO₂ and HNO₃ data from the DC8; the NCAR MOPITT team for the CO satellite data and AEA Technology Environment and DEFRA for the data on the UK National Air Quality Information Archive web site.

References

- Bertschi I.T., D.A. Jaffe, L. Jaegle, H.U. Price and J.B. Dennison (2004), PHOBEA / ITCT 2002 airborne observations of transpacific transport of ozone, CO, volatile organic compounds, and aerosols to the northeast Pacific: Impacts of Asian anthropogenic and Siberian boreal fire emissions, *J. Geophys. Res.*, *109*, D23S12, doi: 10.1029/2003JD004328.
- Bovensmann H., J.P. Burrows, M. Buchwitz, J. Frerick, S. Noel, V.V. Rozanov, K.V. Chance and A.P.H. Goede, (1999), SCIAMACHY – Mission objectives and measurement modes, *J. Atmos. Sci.*, *56*, 127-150.
- Brough N., C.E. Reeves, S.A. Penkett, D.J. Stewart, K. Dewey, J. Kent, H. Barjat, P.S. Monks, H. Ziereis, P. Stock, H. Huntrieser and H. Schlager (2003), Intercomparison of aircraft instruments on board the C-130 and Falcon 20 over Southern Germany during EXPORT 2000', *Atmos. Chem. Phys.*, *3*, 2127-2138, 2003.

Carver G. D., Brown P. D. and Wild O. (1997), The ASAD atmospheric chemistry integration package and chemical reaction database, *Comp. Phys. Commun.*, *105*, 197-215.

Carver G. D. and P. A. Stott (2000), IMPACT: an implicit time integration scheme for chemical species and families, *Ann. Geophys.*, *18*, 337-346.

Cleary P. A., P. J. Wooldridge and R. C. Cohen (2002), Laser-induced fluorescence detection of atmospheric NO₂ with a commercial diode laser and a supersonic expansion, *Appl Opt.*, *41*, 6950-6956.

Damoah R., N. Spichtinger, R. Servranckx, M. Fromm, E. W. Eloranta, I. A. Razenkov, P. James, M. Shulski, C. Forster and A. Stohl (2006), A case study of pyro-convection using a transport model and remote sensing data, *Atmos. Chem. Phys.*, *6*, 173-185.

Drummond J. R. and G. S. Mand (1996), The Measurement of Pollution in the Troposphere (MOPITT) instrument: overall performance and calibration requirements, *J. Atmos. Ocean. Tech.*, *13*, 314-320, 1996.

Duncan B. N., R. V. Martin, A. C. Staudt, R. Yevich, and J. A. Logan (2003), Interannual and seasonal variability of biomass burning emissions constrained by satellite observations, *J. Geophys. Res.*, *108*, D2, 4100, doi:10.1029/2002JD002378.

Duncan B. N., I. Bey, M. Chin, L. J. Mickley, T. D. Fairlie, R. V. Martin and H. Matsueda (2003), 'Indonesian wildfires of 1997: Impact on Tropospheric chemistry', *J. Geophys. Res.*, *108*, D15, 4458, doi: 10.1029/2002JD003195.

Edwards D. P., C. M. Halvorson and J. C. Gille (1999), Radiative transfer modeling of the EOS Terra Satellite Measurement of Pollution in the Troposphere (MOPITT) instrument, *J. Geophys. Res.*, *104*, 16755-16775.

Fehsenfeld F. C. et al. (2006), International Consortium for Atmospheric Research on Transport and Transformation (ICARTT): North America to Europe: Overview of the 2004 summer field study, *J. Geophys. Res.*, (this issue).

Fromm M., R. Bevilacqua, R. Servranckx, J. Rosen, J. P. Thayer, J. Herman and D. Larko (2005), Pyrocumulonimbus injection of smoke to the stratosphere: Observations and impact of the super blowup in northwestern Canada on 3-4 August 1998, *J. Geophys. Res.*, *110*, D12202, doi:10.1029/2005JDD12202.

Gauss M. et al. (2003), Radiative forcing in the 21st century due to ozone changes in the troposphere and the lower stratosphere', *J. Geophys. Res.*, *108*, 4292, doi:10.1029/2002JD002624.

Gerbig C.H., S. Schmitgen, D. Kley, A. Volz-Thomas, K. Dewey and D. Haaks (1999) An improved fast-response VUV resonance fluorescence CO instrument, *J. Geophys. Res.*, *104*, 1699-1704.

Giannakopoulos C., M. P. Chipperfield, K. S. Law and J. A. Pyle (1999), Validation and intercomparison of wet and dry deposition schemes using ²¹⁰Pb in a global three-dimensional off-line chemical transport model, *J. Geophys. Res.*, *104*, 23761-23784.

Green T. J. et al. (2006), An improved dual channel PERCA instrument for atmospheric measurements of peroxy radicals', *J. Environ. Monit.*, (in press).

- Hao W. M. and Liu M. H. (1994), Spatial and Temporal Distribution of Tropical Biomass Burning, *Global Biogeochem. Cy.*, 8, 495-503.
- Holtslag A. A. M. and Boville B. A. (1993), Local versus nonlocal boundary-layer diffusion in a global climate model, *J. Clim.*, 6, 10, 1825-1842.
- Hudman R. C. et al. (2004), Ozone production in transpacific Asian pollution plumes and implications for Ozone air quality in California, *J. Geophys. Res.*, 109, D23S10, doi:10.1029/2004JD004974.
- Kohler I., R. Sausen and R. Reinberger (1997), Contributions of aircraft emissions to the atmospheric NO_x content, *Atmos. Env.*, 31, 1801-1818.
- Law K. S. and Nisbet E. G. (1996), Sensitivity of the methane growth rate to changes in methane emissions from natural gas and coal, *J. Geophys. Res.*, 101, 14387-14397.
- Law K. S., Law, K. S., P. H. Plantevin, D. E. Shallcross, H. L. Rogers, J. A. Pyle, C. Grouhel, V. Thouret and A. Marenco, (1998), Evaluation of modeled O₃ using MOZAIC data, *J. Geophys. Res.*, 103, 25721-25737.
- Law K. S., P.-H. Plantevin, V. Thouret, A. Marenco, W. A. H. Asman, M. Lawrence, P. J. Crutzen, J.-F. Muller, D. A. Hauglustaine and M. Kanakidou (2000), Comparison between global chemistry transport model results and Measurement of Ozone and Water Vapor by Airbus In-Service Aircraft (MOZAIC) data, *J. Geophys. Res.*, 105, 1503-1525.

McKeen S. A., G. Wotawa, D. D. Parrish, J. S. Holloway, M. P. Buhr, G. Hübler, F. C. Fehsenfeld, and J. F. Meagher (2002), Ozone production from Canadian wildfires during June and July of 1995, *J. Geophys. Res.*, *107*, 4192, doi:10.1029/2001JD000697.

Methven J. S. R. Arnold, F. M. O'Connor, H. Barjat, K. Dewey, J. Kent and N. Brough (2003), Estimating photochemically produced ozone throughout a domain using flight data and a lagrangian model, *J. Geophys. Res.*, *108*, 4271, doi:10.1029/2002JD002955.

Methven J. et al. (2006), Establishing Lagrangian connections between observations within air masses crossing the Atlantic during the ICARTT experiment, *J. Geophys. Res.*, 2006 .

Müller J. F. (1992), Geographical distribution and seasonal variation of surface emissions and deposition velocities of atmospheric trace gases, *J. Geophys. Res.*, *97*, 3787-3804.

F. M. O'Connor, G. D. Carver, N. H. Savage, J. A. Pyle, J. Methven, S. R. Arnold, K. Dewey and J. Kent (2005), Comparison and visualisation of high-resolution transport modeling with aircraft measurements, *Atm. Sci. Lett.*, *6*, 164-170, doi: 10.1002/asl.111.

O'Connor F. M., K. S. Law, J. A. Pyle, H. Barjat, N. Brough, K. Dewey, T. Green, J. Kent, and G. Phillips (2004), Tropospheric Ozone Budget: Regional and Global Calculations, *Atmos. Chem. Phys. Discuss.*, *4*, 991-1036.

Pfister G. P. G. Hess, L. K. Emmons, J.-F. Lamarque, C. Wiedinmyer, D. P. Edwards, G. Pétron, J. C. Gille and G. W. Sachse (2005), Quantifying CO emissions from the 2004 Alaskan Wildfires using MOPITT CO data, *Geophys. Res. Lett.*, *32*, L11809, doi: 10.1029/2005GL022995, 2005.

Piccot S. D. , J.J. Watson and J.W. Jones (1992), A global inventory of volatile organic compound emissions from anthropogenic sources, *J. Geophys. Res.*, *97*, 9897-9912.

Prather, M. J. (1986), Numerical advection by conservation of second-order moments, *J. Geophys. Res.*, *91*, 6671-6681.

Price C. and Rind D. (1992), 'A simple lightning parameterization for calculating global lightning distributions', *J. Geophys. Res.*, *97*, 9919-9933.

Richter A. and Burrows J. P. (2002), Retrieval of tropospheric NO₂ from GOME measurements, *Adv. Space Res.*, *29*, 1673-1683.

Richter A., J.P. Burrows, H. Nüß, C. Granier and U. Niemeier (2005), Increase in tropospheric nitrogen dioxide over China observed from space, *Nature*, *437*, 129-132, doi:10.1038/nature04092.

Savage N. H. , Law, K. S., Pyle, J. A., Richter, A., Nüß, H. and Burrows, J. P. (2004), Using GOME NO₂ satellite data to examine regional differences in TOMCAT model performance, *Atmos. Chem. Phys.*, *4*, 1895-1912.

Schlager H., P. Schulte, F. Flatoy, F. Slemr, P. van Velthoven, H. Ziereis and U. Schumann (1999), Regional nitric oxide enhancements in the North Atlantic flight corridor observed and modeled during POLINAT 2 – a case study, *Geophys. Res. Lett.*, *26*, 3061-3064.

Schultz, MG., A. Heil, J.J. Hoelzemann, A. Spessa, A., K. Thonicke, J. Goldammer, A.C. Held. and J.M. Pereira (2006), Global emissions from Vegetation fires from 1960 to 2000. *Glob. Biogeochem. Cycles*, *Submitted*.

Singh H. B. et al. (2006), Overview of the summer 2004 Intercontinental Chemical Transport Experiment – North America (INTEX-A), *J. Geophys. Res.*, (this issue).

Stockwell D. Z., M. A. Kritz, M. P. Chipperfield, and J.A. Pyle (1998), Validation of an off-line three-dimensional chemical transport model using observed Radon profiles – 2. Model results', *J. Geophys. Res.*, *103*, 8433-45.

Stockwell D. Z., C. Giannakopoulos, P. -H. Plantevin, G. D. Carver, M. P. Chipperfield, K. S. Law, J. A. Pyle, D. E. Shallcross and K. -Y. Wang (1999), Modelling NO_x from lightning and its impact on global chemical fields, *Atmos. Env.*, *33*, 4477-4493.

Tiedke, M. (1989), A comprehensive mass flux scheme for cumulus parameterization in large-scale models, *Mon. Weather Rev.*, *117*, 1779-1800.

Turquety S. et al. (2006), Inventory of boreal fire emissions for North America in 2004: the importance of peat burning and pyro-convective injection, *J. Geophys. Res.*, (this issue).

Wang, K. Y., J.A. Pyle, J.A. and C. Bridgeman (1999), Implementation of a convective atmospheric boundary layer scheme in a tropospheric chemistry transport model, *J. Geophys. Res.*, *104*, 23729-23745.

Whalley L. K. A.C. Lewis, J.B. McQuaid, R.M. Purvis, J.D. Lee, K. Stemmler, C. Zellweger and P. Ridgeon (2004), Two high-speed, portable GC systems designed for the measurement of non-methane hydrocarbons and PAN: Results from the Jungfraujoch High Altitude Observatory, *J. Environ. Monit.*, *6*, 234-241.

Wild O., K. S. Law, D. S. McKenna, B. J. Bandy, S. A. Penkett and J. A. Pyle (1996), Photochemical trajectory modeling studies of the North Atlantic region during August 1993, *J. Geophys. Res.*, *101*, 29,269-29,288.

Wofsy S. C., G. W. Sachse, G. L. Gregory, D. R. Blake, J. D. Bradshaw, S. T. Sandholm, H. B. Singh, J. A. Barrick, R. C. Harriss, R. W. Talbot, M. A. Shipham, E. V. Browell, D. J. Jacob and J. A. Logan (1992), Atmospheric Chemistry in the Arctic and Subarctic: Influence of Natural Fires, Industrial Emissions, and Stratospheric Inputs, *J. Geophys. Res.*, *97*, 16731-46.

Wotawa G. and Trainer M. (2000), The Influence of Canadian Forest Fires on Pollutant Concentrations in the United States, *Science*, *288*, 324-328.

Yevich R. and Logan J. A. (2003), An assessment of biofuel use and burning of agricultural waste in the developing world, *Global Biogeochem. Cycles*, *17*, 1095, doi:10.1029/2002GB001952.

TABLE 1: THE FOUR MODEL SIMULATIONS	
A	No biomass burning (BB) emissions from Alaska and west Canada
B	Alaska and west Canada BB emissions put in between surface and 260 hPa
C	“Pyro-convective” vertical mixing of BB emissions and O ₃ over Alaska and west Canada
D	“Pyro-convective” vertical mixing and low NO _x BB emissions over Alaska and west Canada

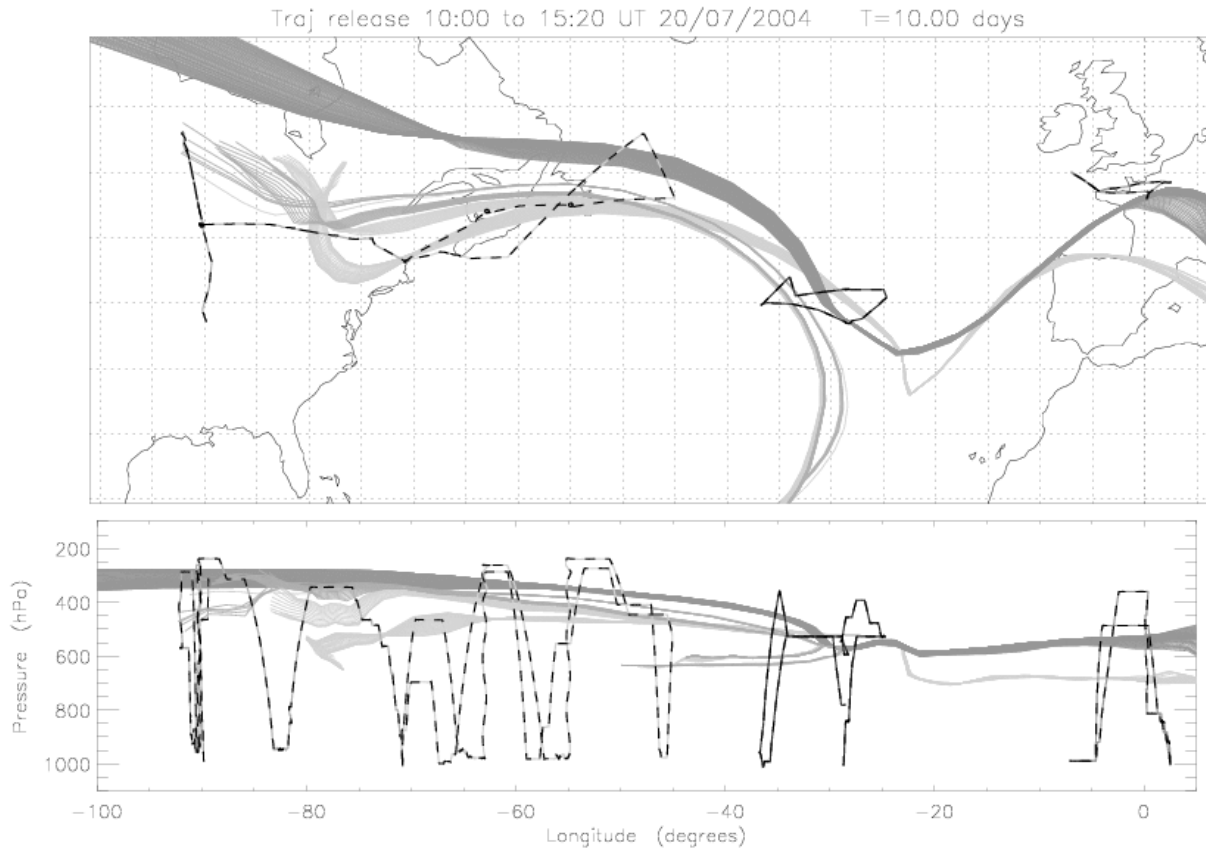


Figure 1. From Methven et al. 2006, the 3D trajectory of the large fire plume over several days (dark lines, the lighter lines are other air mass trajectories), intercepted by the DC8 over the eastern USA on the 18th July 2004, by the BAe-146 in the mid Atlantic on the 20th and by the DLR Falcon over western Europe on the 23rd. The locations of the three flight tracks are shown by the dashed lines.

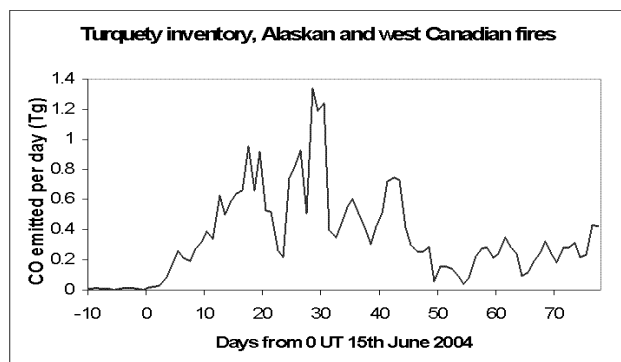


Figure 2: The emission of CO from the Alaskan and west Canadian fires during June to August 2004, from the Turquety et al. (2006) daily inventories of biomass burning.

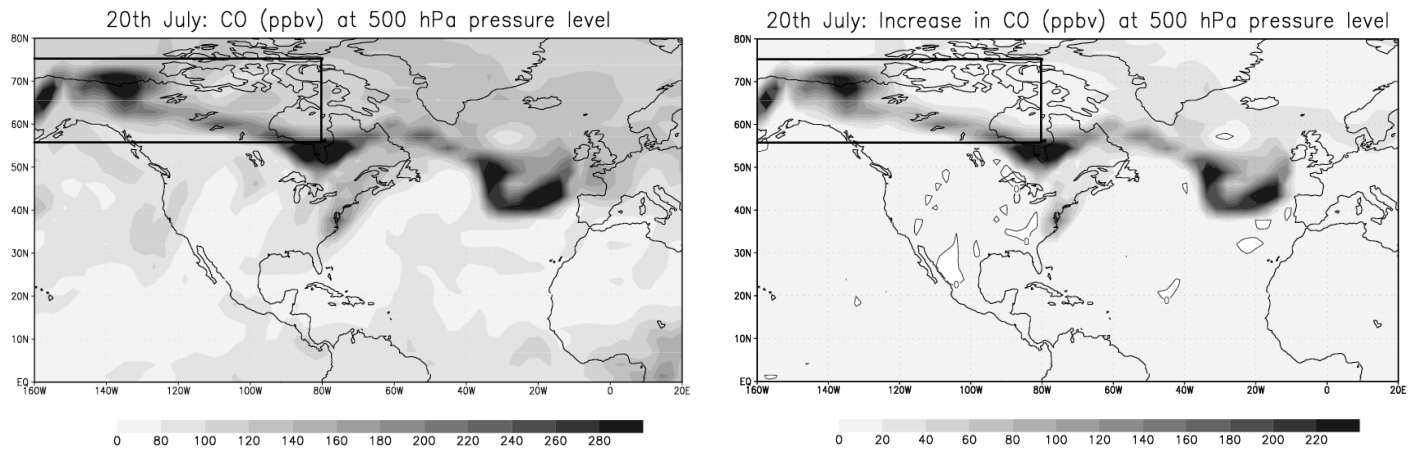


Figure 3. p-TOMCAT tracer field of CO from run D (left) and the increase between runs A and D (right), at 500 hPa on the 20th July 2004 (12:00 UT). The box represents the region in which the small areas of biomass burning emissions were treated differently between the model simulations.

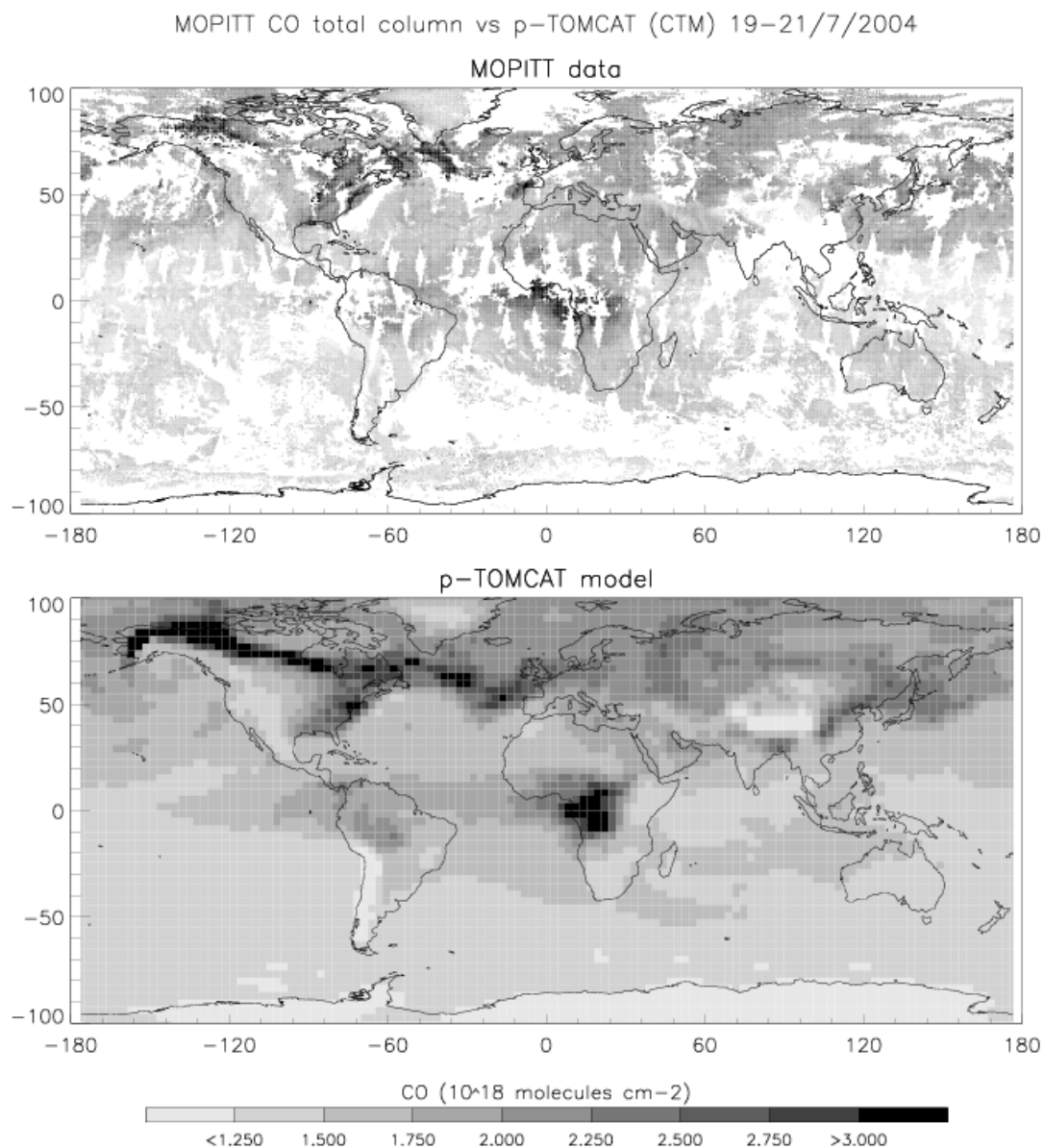


Figure 4. Measurements of CO columns from MOPITT during the 19th, 20th and 21st July 2004, compared to p-TOMCAT results from run D. The grayscale bar is the same for both plots (10^{18} molecules cm^{-2}).

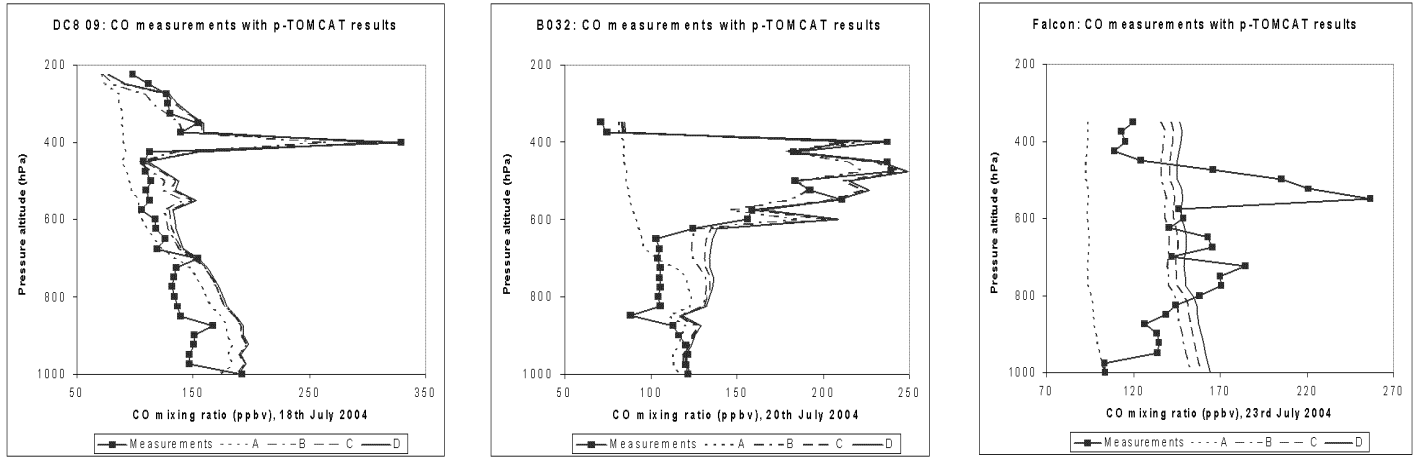


Figure 5. Measurements of CO (ppbv) vs pressure altitude (hPa) from DC8 flight 09 on the 18th July 2004, BAe-146 flight B032 on the 20th July and the DLR Falcon flight on the 23rd, along the flight tracks shown in figure 1, with p-TOMCAT results from the four simulations.

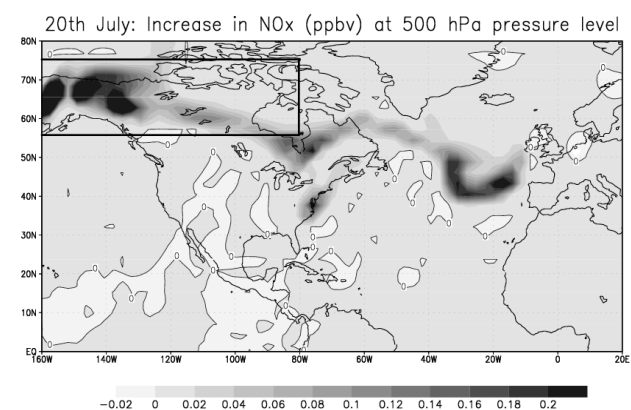
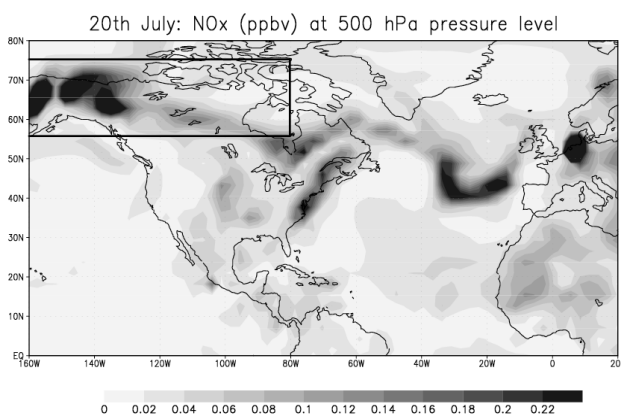
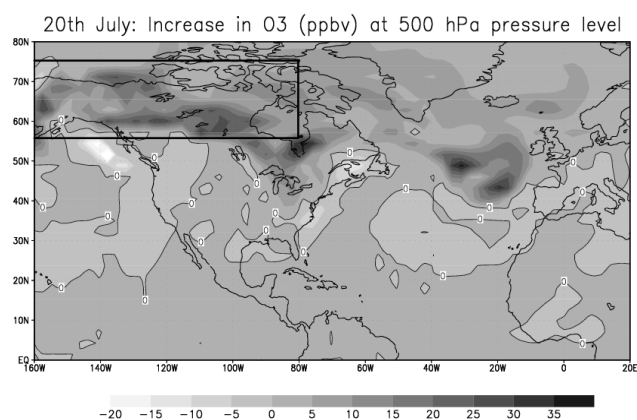
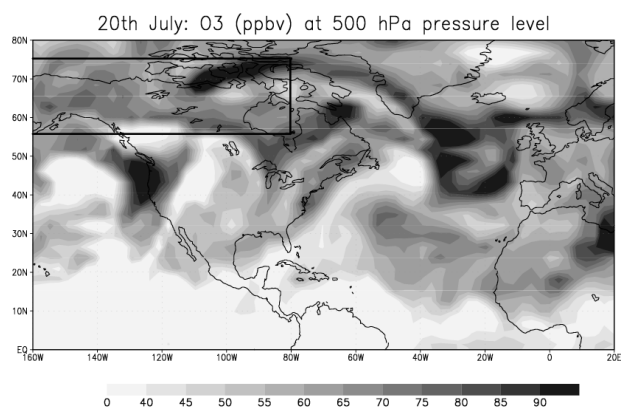


Figure 6. p-TOMCAT tracer fields of O₃ and NO_x (ppbv) from run D (left) and the increases between runs A and D (right) at 500 hPa on the 20th July 2004 (12:00 UT). The box represents the region in which the small areas of biomass burning emissions were treated differently between the model simulations.

SCIAMACHY NO₂ Tropospheric column vs p-TOMCAT (CTM) 19–21/7/2004

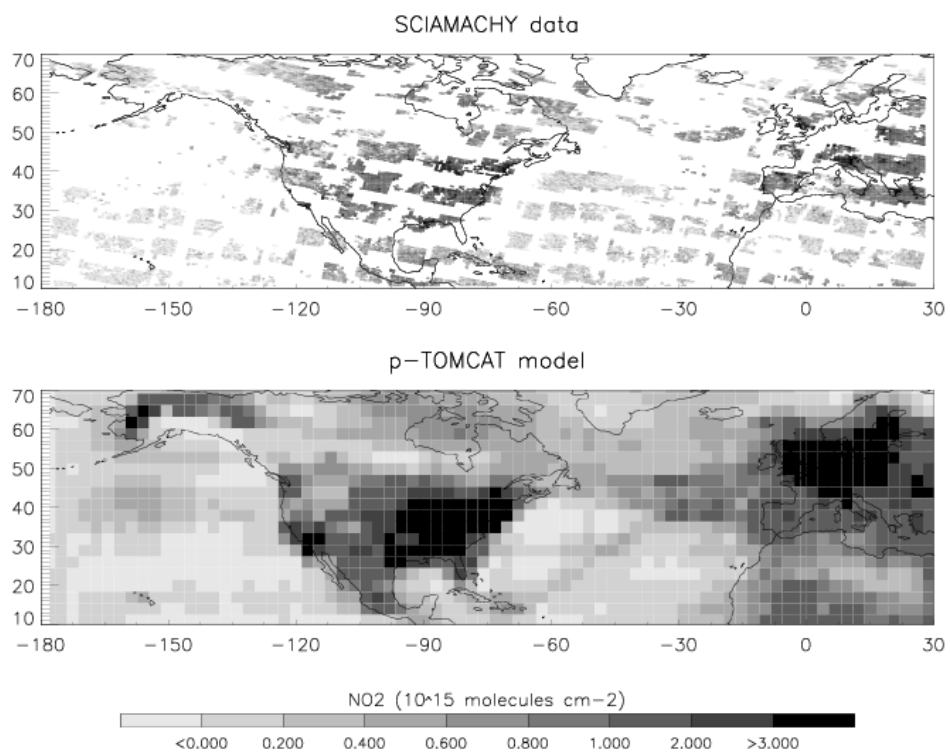
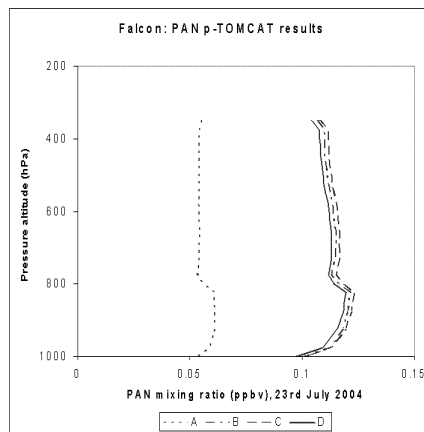
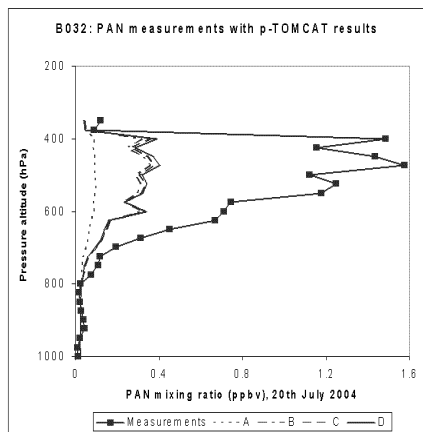
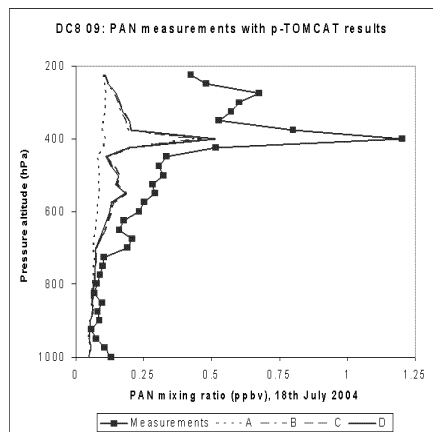
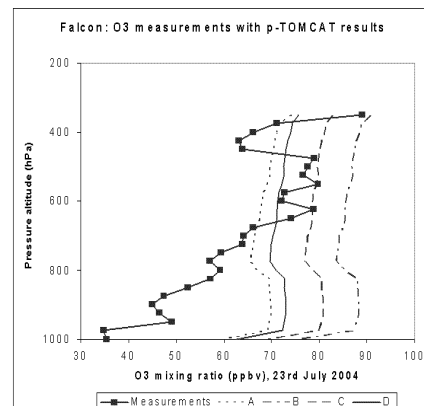
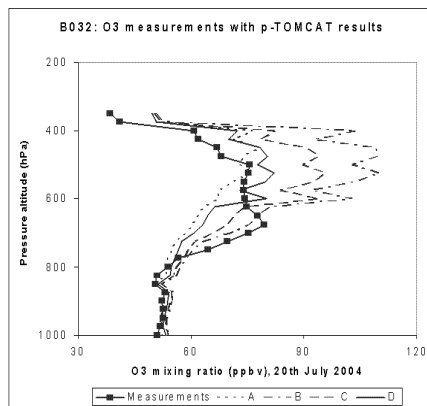
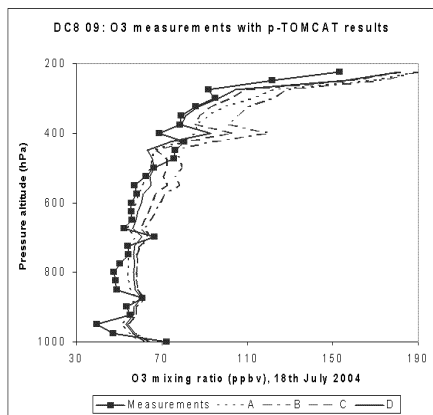
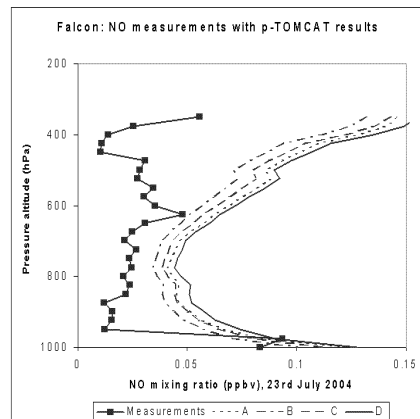
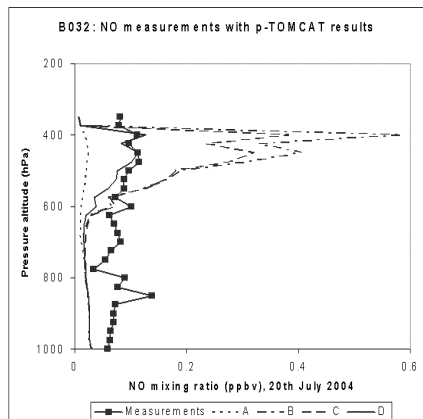
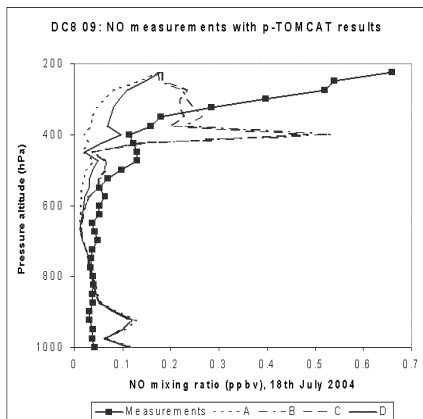


Figure 7. Measurements of NO₂ tropospheric columns from SCIAMACHY during the 19th, 20th and 21st July 2004, compared to p-TOMCAT results from run D. Same grayscale bar for both plots (10^{15} molecules cm^{-2}).



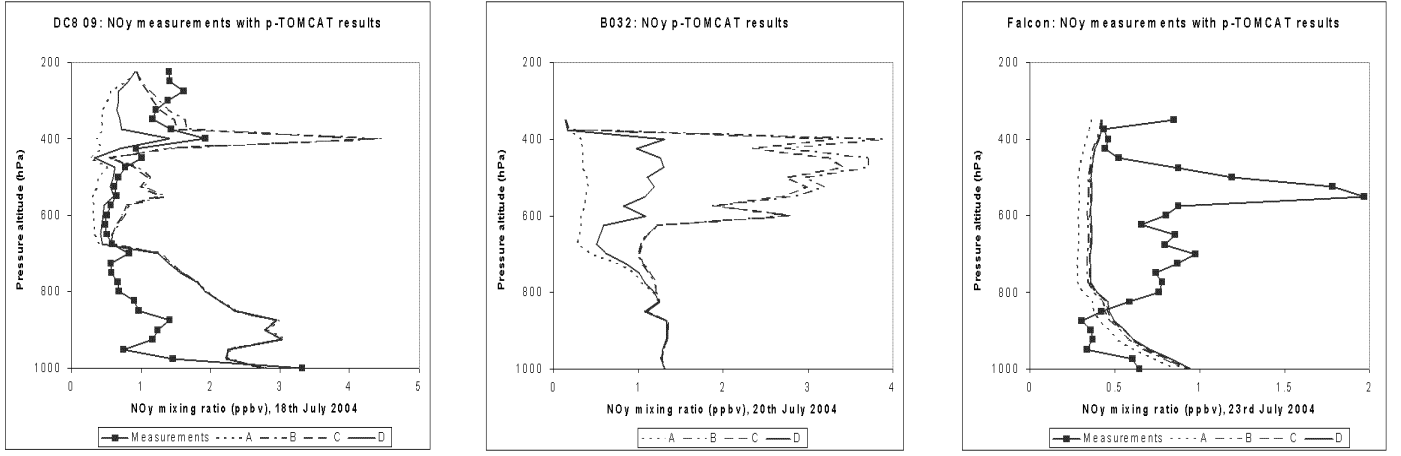


Figure 8. Measurements of NO, O₃, PAN and NO_y (ppbv) vs pressure (hPa) from DC8 flight 09 on the 18th July 2004, BAe-146 flight B032 on the 20th and the DLR Falcon flight on the 23rd, along the flight tracks shown in figure 1, with p-TOMCAT results from the four simulations.

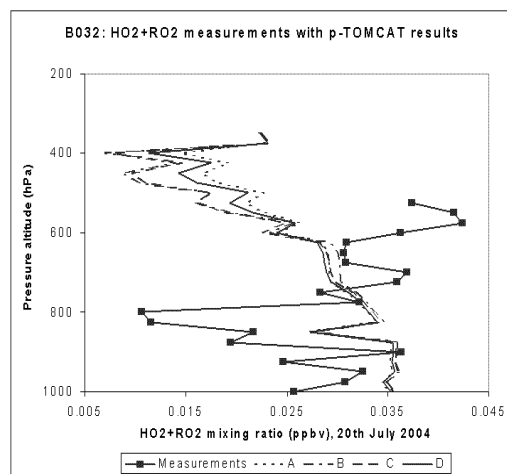
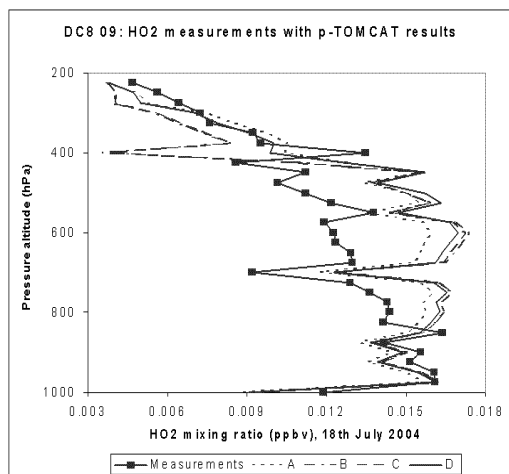


Figure 9. Peroxy Radicals (ppbv) plotted against pressure altitude (hPa) from DC8 flight 09 on the 18th July 2004 and from BAe-146 flight B032 on the 20th, with p-TOMCAT results from the four simulations.

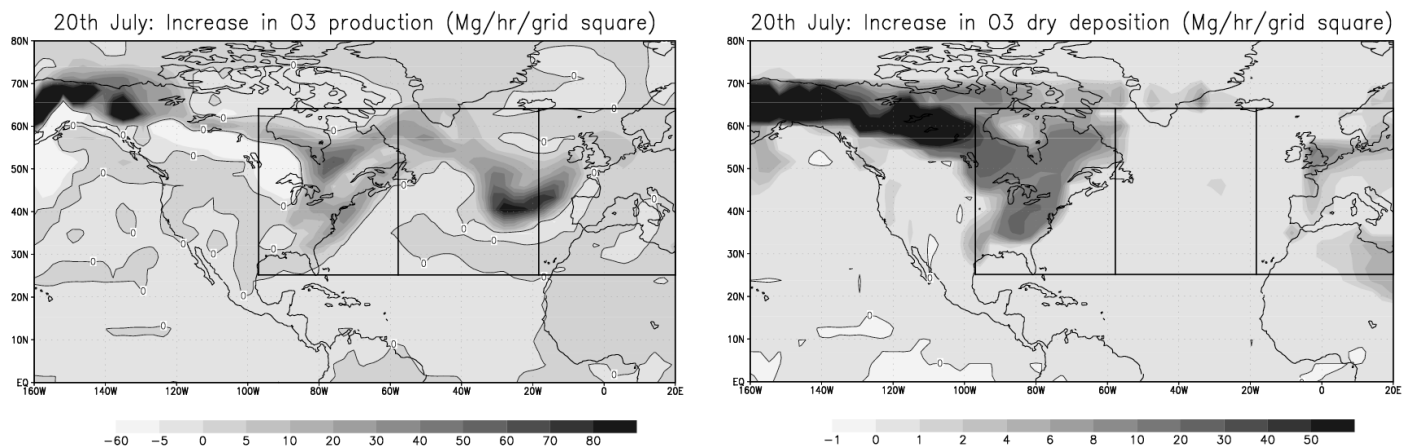


Figure 10. Difference in O₃ net chemical production and dry deposition (Mg/hr/2.8° x 2.8° grid square), increase between model runs A and D within the model troposphere during the 20th July 2004. The rectangles show the eastern USA, mid Atlantic and western Europe regions.

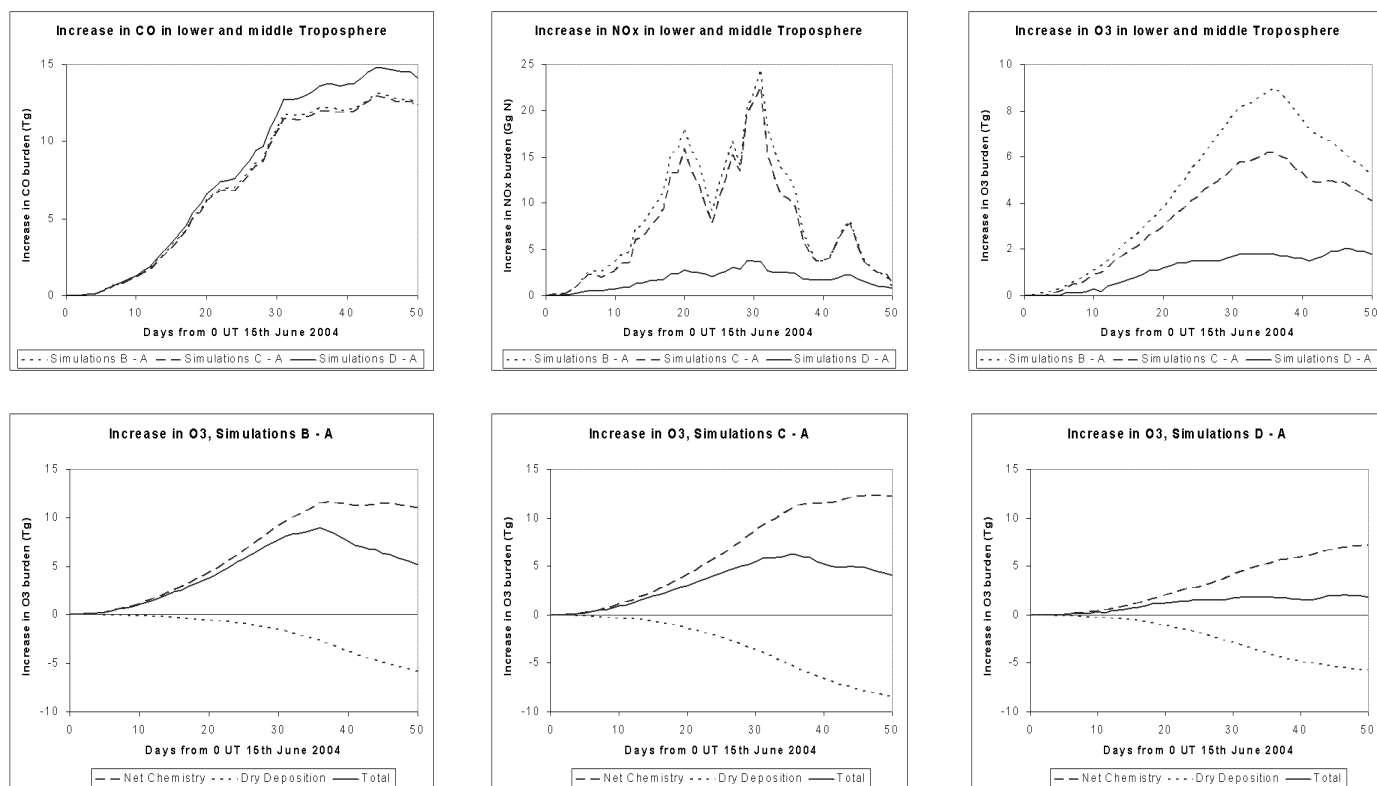


Figure 11. The top panels show the increased CO (Tg), NO_x (Gg N) and O₃ (Tg) within the model northern hemisphere lower and middle troposphere between run A and runs B, C and D over 50 days from 15th June 2004 (0:00 UT). The bottom panels show the increased O₃ (Tg) from net chemistry and loss from dry deposition (with the increased burden) between the different model simulations over the 50 days.

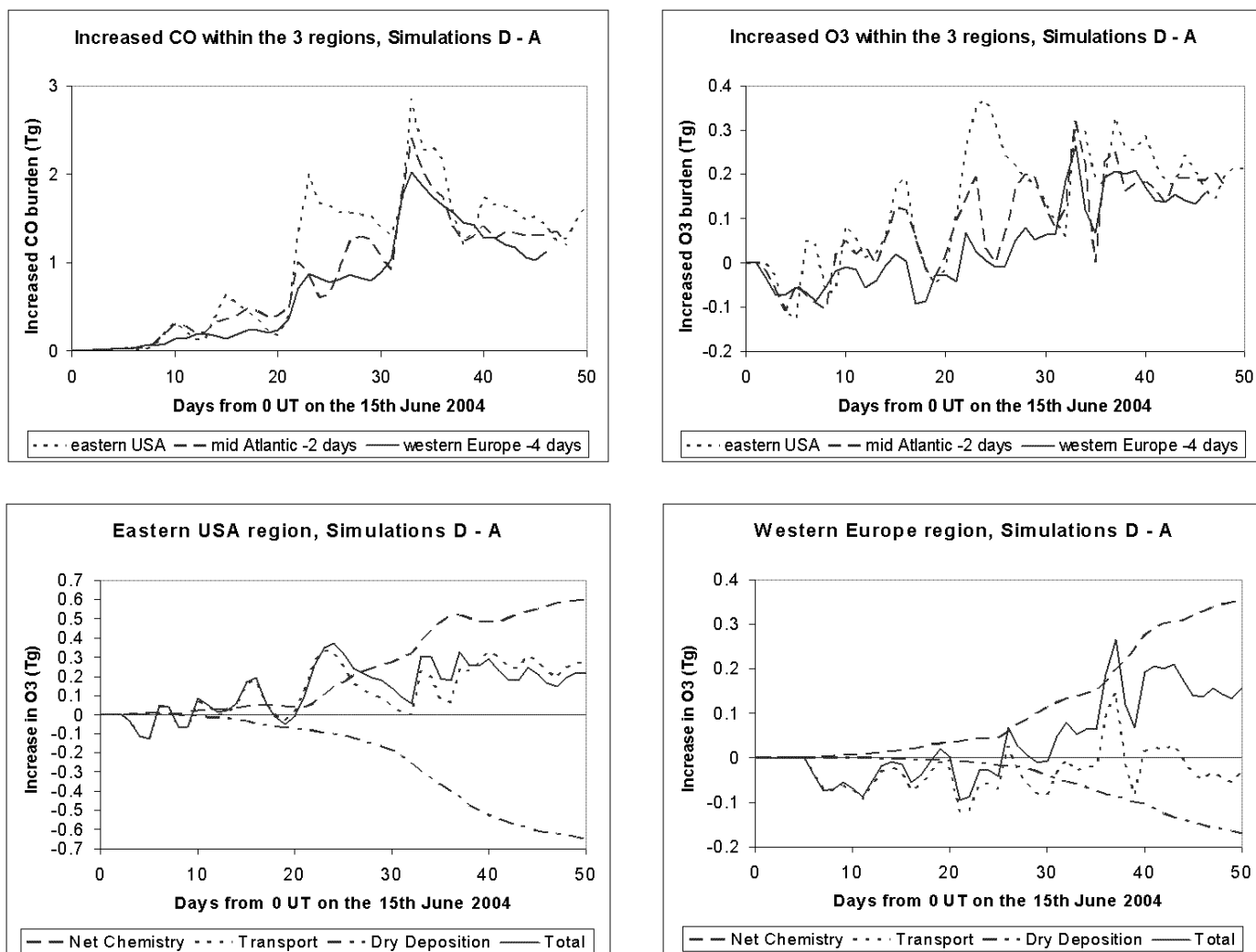


Figure 12. The top panels show the increase in model CO and O₃ (Tg) within 3 regions of the lower and middle troposphere, between runs A and D during 50 days from 15th June 2004 (0:00 UT), mid Atlantic lines are shifted by 2 days and western Europe lines by 4 days to remove the 2 day time lag between the regions. The bottom panels show the increase in model O₃ (Tg) within the eastern USA and western Europe regions, between runs A and D during the 50 days, due to different processes: net chemistry, transport from/to other regions and dry deposition (with the increased burden).

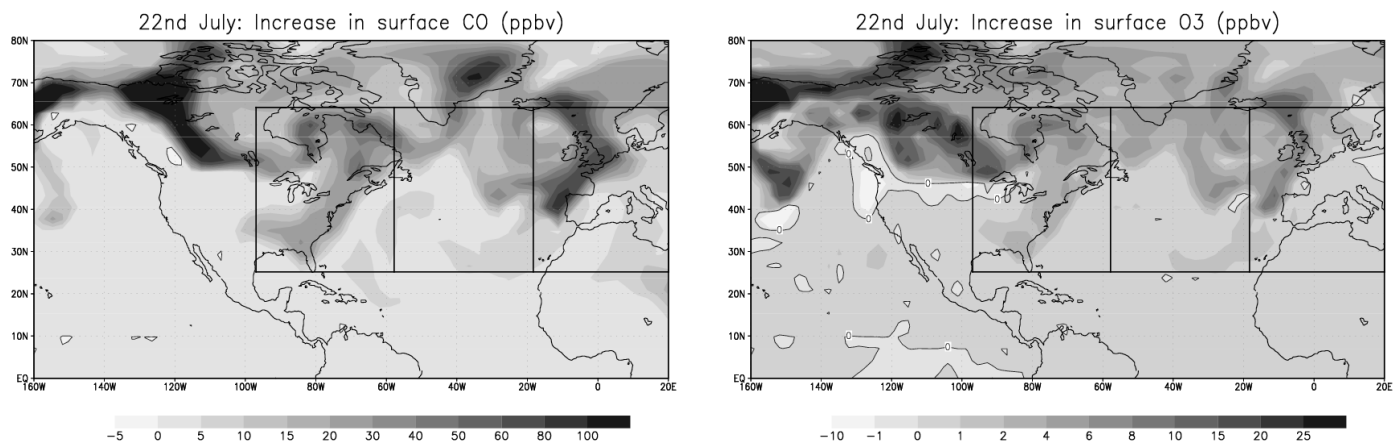


Figure 13. Difference in surface CO and O₃ (ppbv) on the 22nd July 2004 (12:00 UT), between runs A and D.

The rectangles show the eastern USA, mid Atlantic and western Europe regions.

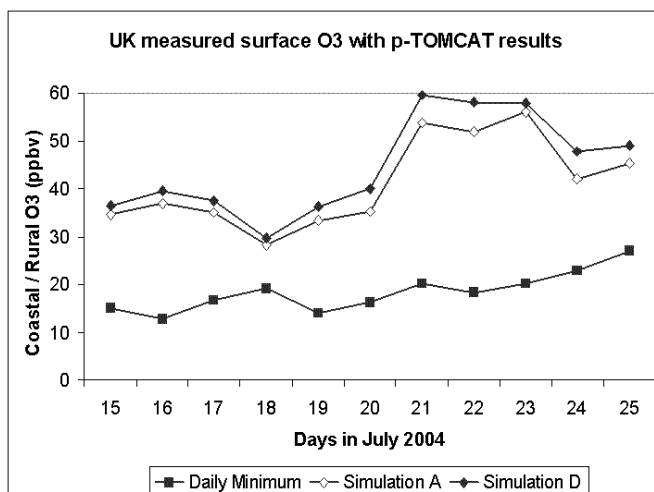
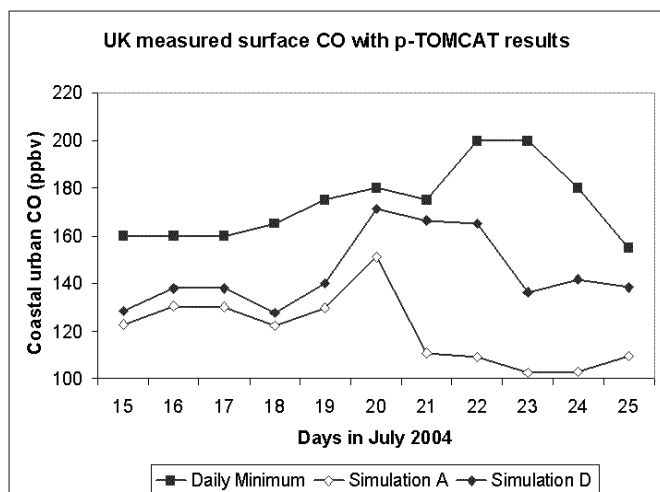


Figure 14. Daily minimum surface measurements of CO and O₃ (ppbv) for the UK during July 2004 (values from 16 coastal urban sites and 15 coastal and rural sites across the UK), with model values across the UK from runs A and D (the region covering 7.0° W-1.4° E, and 50.4°-58.8° N) at 12:00 UT on each day.